

Electrically modulated capillary filling imbibition of nematic liquid crystals

Jayabrata Dhar and Suman Chakraborty*

Indian Institute of Technology Kharagpur, Kharagpur 721302, India

(Received 25 January 2018; revised manuscript received 15 March 2018; published 9 April 2018)

The flow of nematic liquid crystals (NLCs) in the presence of an electric field is typically characterized by the variation in its rheological properties due to transition in its molecular arrangements. Here, we bring out a nontrivial interplay of a consequent alteration in the resistive viscous effects and driving electrocapillary interactions, toward maneuvering the capillary filling dynamics over miniaturized scales. Considering a dynamic interplay of the relevant bulk and interfacial forces acting in tandem, our results converge nicely to previously reported experimental data. Finally, we attempt a scaling analysis to bring forth further insight to the reported observations. Our analysis paves the way for the development of microfluidic strategies with previously unexplored paradigms of interaction between electrical and fluidic phenomenon, providing with an augmented controllability on capillary filling as compared to those reported to be achievable by the existing strategies. This, in turn, holds utilitarian scopes in improved designs of functional capillarities in electro-optical systems, electrorheological utilities, electrokinetic flow control, as well as in interfacing and imaging systems for biomedical microdevices.

DOI: [10.1103/PhysRevE.97.043107](https://doi.org/10.1103/PhysRevE.97.043107)**I. INTRODUCTION**

Flow actuation and transport characteristics of ordered nematic liquid crystals (NLCs) in a microfluidic environment are extremely significant toward the understanding of intriguing topological structures and flow modulation [1,2], besides having a wide extent of applications ranging from electro-optical systems [3–5], electrorheological utilities [6–10], electrokinetic flow control [11,12] to biomedical devices [13–15]. These problems are invariably characterized by an intrinsic coupling of the inherent topological features, the effects of multiple confining interfaces, and the anisotropic viscous characteristics [16,17].

Electrocapillarity [18] of NLCs exhibits interesting flow characteristics on account of the coupling between the flow-induced rheological variation, electrocapillary (E_c) effects, and electrorheological (ER) phenomenon [9,19]. Such concurrent confluence of the interfacial and electrical influences to modulate microscale flow of NLCs is by no means trivial, but is yet to be effectively utilized by the applied research community toward obtaining augmented functionalities by exploiting the underlying capillary filling characteristics.

By exploiting such significant interconnections between the driving and resisting forces, here we bring out a yet-unexplored paradigm of achieving capillary imbibition of NLCs with augmented modulation capabilities, with electric field and interfacial conditions being employed as intrinsically tunable parameters. We explain the physical mechanism behind this paradigm of electrocapillarity of NLCs and provide a design basis that paves the way for the development of microfluidic pathways with an additional degree of freedom provided toward modulating rates of capillary filling as compared to

those reported to be achievable by the existing microfluidic strategies.

II. THEORETICAL FRAMEWORK

NLCs exhibit a sense of directionality maintained by their constituent rod-shaped molecules that impart the medium its intrinsic anisotropic characteristics. A unit director vector \mathbf{n} , that denotes the localized average direction of the nematic molecules, is used to represent their long-range orientational order [20]. Essentially, the framework describing the transients of the capillary front (meniscus) of NLCs follow from the coupled interplay among the viscous, inertial, electrical, gravitational, nematic-isotropic interfacial, and surface tension effects [21], leading to a lumped force balance analysis [22–24]. Such reduced-order approach has been successful in predicting experimental observation to appreciable accuracy [25–28], despite its inherent limitation to capture the exact meniscus shape. The present formalism additionally captures the issues involving anisotropic viscosity, coupling between the director configuration with flow field and variable anchoring at the nematic-isotropic interface and significantly improves on a previously tackled study [29]. Further, the electric-field-induced electrocapillarity and the intrinsic ER behavior exhibited by the NLC medium are also addressed. A comparison with previous experiments along with a detailed scaling analysis of the developed formalism bring forth better understanding to our reported observations.

We consider an anisotropic NLC medium having density ρ being sucked into a parallel-plate channel of width $2H$ by the action of electrocapillary and nematic forces (Fig. 1). The coordinate origin is considered at the channel center while x and y denote the axial and transverse coordinates, respectively. The medium elasticity is characterized by an elastic constant K . An electric field of magnitude E is applied transverse to the capillary rise. Dielectric constants of the

*Corresponding author: suman@mech.iitkgp.ernet.in

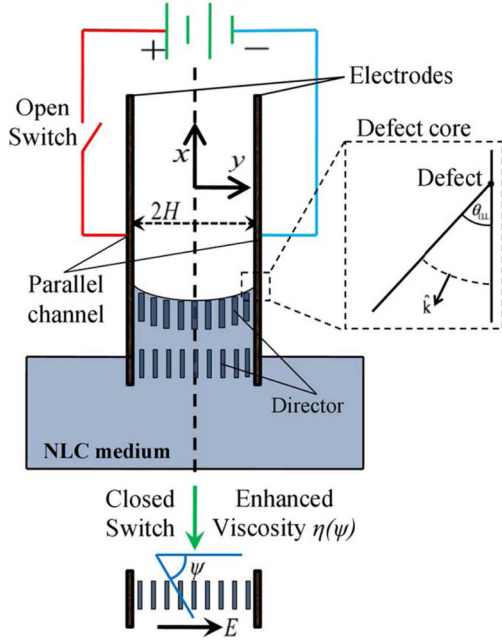


FIG. 1. Schematic of the setup for electrocapillary imbibitions of NLC medium rising through a parallel-plate channel. The viscosity variation is the manifestation of different director configurations for open- and closed-switch conditions. Inset: The topological defect is situated at the contact line that demarcates the solid (S), nematic (N), and vapor (V) phases. The defect core has a radius (r_c) in order of molecular dimensions (hence not shown in the figure) and a normal $\hat{\mathbf{k}}$.

nematic medium parallel and perpendicular to the director are ε_{\parallel} and ε_{\perp} , respectively. At the interface, the constant NV isotropic contact angle is denoted by θ_c and the surface tension is denoted by γ_s . We invoke the classical Ericksen-Leslie-Parodi (ELP) formalism with first-order Oseen-Frank elasticity to investigate the dynamics of the nematic fluid [30].

For the dynamics described above, we account for the balance among the inertial, viscous F_{visc} , surface tension F_{surf} , nematic F_{NLC} , and gravitational F_{grav} forces (defined per unit breadth) as

$$\frac{d}{dt} \left(2H\rho x \frac{dx}{dt} \right) = F_{\text{surf}} + F_{\text{NLC}} - F_{\text{grav}} - F_{\text{visc}} \quad (1)$$

with t representing time. We begin by identifying each of the lumped forces involved in the capillary filling process. The gravitational force per unit breadth for a liquid rise is straightforward and is given by $F_{\text{grav}} = 2\rho g H x$ where g is acceleration due to gravity. Here the density of the vapor phase is neglected for such reduced-order framework approach. For nematics, the surface tension force, nematic-isotropic interfacial induced force, and viscous force, however, need involved attention and are detailed below.

A. Interfacial elastoelectric effects

The genesis of interfacial elastic effects for NLCs is attributed to the director deformations adjacent to the nematic-vapor interface [31] and is responsible for the altered Jurin height observed in a capillary rise experiment [32]. The modified contact angle accounting for the interfacial elasticity

of NLCs is obtained from the balance of surface and bulk stresses as

$$\gamma_s^{\text{NV}} \cos \theta - \hat{\mathbf{e}}_x \cdot \oint_{\text{Core}} \hat{\mathbf{k}} \cdot \mathbf{t}_b dl + \gamma_s^{\text{SN}} - \gamma_s^{\text{SV}} = 0, \quad (2)$$

where \mathbf{t}_b is the bulk elastic stress of the nematic given by $K(\nabla \mathbf{n}) : (\nabla \mathbf{n})^T$ assuming one-constant approximation and the rest of the symbols are detailed in Fig. 1. As a representative case, we focus on the capillary rise of NLC 5CB (4-cyano-4'-pentylbiphenyl) rising through a glass channel. 5CB is known to achieve a strong planar anchoring of its director at the glass walls [1] while at the free surface, the director arranges in a homeotropic configuration [33].

Here, we must comment that one-constant approximation for NLC elastic energy has been used previously in numerous studies. Such consideration avoids unnecessary computational complexities while maintaining a certain degree of accuracy that is required to understand the transport process in realistic conditions [20,30,34–36]. In fact, relaxing the one-constant approximation will render the problem analytically intractable besides hardly bringing about any change to the observed electrocapillary and ER behavior relevant to the focus of this study. Now from the above stress balance, a scaling analysis reveals the modified contact angle as [31]

$$\gamma_{s,\parallel\perp}^{\text{NV}} \cos \theta_{\parallel\perp} - \frac{K}{2r_c} \varphi_{E,\parallel\perp}^2 \sin \theta_{\parallel\perp} = \gamma_{s,\text{iso}}^{\text{SV}} - \gamma_{s,\parallel\perp}^{\text{SN}}, \quad (3)$$

where $\varphi_{E,\parallel\perp} = [(\pi/2) - \theta_{\parallel\perp}]/(\pi - \theta_{\parallel\perp})$ and $\gamma_{s,\parallel\perp}^{\text{NV}} = \gamma_{s,\text{iso}}^{\text{NV}} + \gamma_{s,\text{an}}^{\text{NV}}/2$ and $\gamma_{s,\parallel\perp}^{\text{SN}} = \gamma_{s,\text{iso}}^{\text{SN}}$ [31]. Here the subscript $\parallel \perp$ denotes the modified surface tension due to strong planar-homeotropic anchoring at the NS - NV interfaces while iso states the isotropic counterpart of them. Such a scenario of strong (or hard) anchoring at the channel walls has been experimentally achieved in many instances in microchannel flows. Any desired director orientation at the boundaries can be induced through physicochemical processes [2,37,38]. The implication of such director control to obtain different director combinations at the NS - NV interfaces will be further discussed later to build on the concept of better controllability of these systems. For these other generalized anchoring possibilities, a similar stress balance may be applied to obtain the corresponding modified contact angles. Besides, since director anchoring energy is much less than the surface energy (i.e., $\gamma_{s,\text{an}}^{\text{NV}} \ll \gamma_{s,\text{iso}}^{\text{NV}}$) [31], we consider $\gamma_{s,\parallel\perp}^{\text{NV}} \approx \gamma_{s,\text{iso}}^{\text{NV}}$ throughout this study. We note that the surface tension at the SV interface is always isotropic [Eq. (3)] as the vapor lacks any elastic properties like the NLC medium. Another aspect that comes to our attention is the modification in Young's equation [Eq. (3)] due to nucleation of a topological defect. Topological defects may either arise due to geometrical constraints in the nematic phase or get induced due to NLC flows that are driven by external agents [20,39,40]. Since we are primarily concerned with low Er value flows, flow-induced topological defects inherent to NLC medium remain absent [41–43] and the flow may be considered “elastically laminar.” Therefore, here we concentrate on topological defects arising out of geometrical constraints. In this case, these defects occur either at the contact line or close to the contact line and are dictated by the anchoring at the NS and NV interfaces. In the present scenario for 5CB with planar anchoring at the capillary walls and homeotropic anchoring at the NV interface,

a defect appears at the contact line [31] as these surfaces are not parallel to each other. The defect at the contact line affects the energy of the system and apparently changes the effective surface energy balance, thus rendering a modified form of the Young's equation as stated above. Due to this modification, the driving force also gets altered, which results in the alteration of the capillary filling hydrodynamics. One can make an obvious deduction that in the absence of any associated elastic or anchoring energies and defect formation (i.e., an isotropic case), one gets back the classical Young's equation $\gamma_{s,iso}^{SV} - \gamma_{s,iso}^{SN} = \gamma_{s,iso}^{NV} \cos \theta_c$.

On the other hand, the electric field influence on the contact angle is expressed through the Young-Lippmann (YL) equation [28] as

$$\cos \theta_{Ec} = \cos \theta_c + \frac{\varepsilon_0 \bar{\varepsilon} H E^2}{w_c \gamma_{s,iso}^{NV}}, \quad (4)$$

where w_c is the contribution factor (which has an order of magnitude of 10), θ_{Ec} is the electrocapillary modified contact angle, ε_0 is the permittivity of free space, and $\bar{\varepsilon}$ is the effective permittivity of the NLC medium. As a first approximation, we have assumed a constant electric field within the NLC domain. Consideration of a constant transverse electric field is common to NLC studies dealing with ER phenomena [7–9,44,45]. The variation in the field due to director distortions for such cases negligibly affects the effective ER behavior and the resulting capillary filling rates. Further, the exclusion of ionic presence and conductivity anisotropy in the system has also been a commonly considered assumption for NLCs like 5CB [8,45,46]. Although strictly speaking, 5CB has small conductivity anisotropy, here we neglect that assumption on the basis of a first approximation and focus our study primarily on the filling dynamics of the problem. Again, for problems involving applied transverse electric field, the result obtained via the consideration of these assumptions does not deviate much from the case when these assumptions are relaxed. Finally, in order to account for the coupled effect of excess nematic elasticity and electric-field-induced surface energy, here we modify the YL due to extra bending influence at the NV interface and propose an effective contact angle

$$\cos \theta_{\perp\perp} - \frac{K}{2\gamma_{s,iso}^{NV} r_c} \varphi_{E,\perp\perp}^2 \sin \theta_{\perp\perp} = \cos \theta_{Ec}. \quad (5)$$

Thus, from a given θ_c , the effective contact angle $\theta_{\perp\perp}$ is obtained from YL form, Eqs. (4) and (5). The modified interfacial force per unit breadth thus reads $F_{surf} = 2\gamma_{s,iso}^{NV} \cos \theta_{\perp\perp} + (K C_{\perp\perp}/H)$ where the parameter $C_{\perp\perp}$ is in the order of unity.

B. Anisotropic viscous effects

The estimation for viscous force, which shares its concepts from the reduced-order approach [47–49] and the ELP formalism [30], must follow from coupling of fluid rheology and director configuration that facilitates the capturing of the inherent anisotropy in NLC medium. In view of the reduced-order approach, we appeal to the steady Cauchy's equation for a Poiseuille flow confined in a parallel microchannel (d/dy)(T_{12}) = $-a_p$ where a_p is the pressure gradient, T_{12} is the relevant shear stress, and the capillary velocity reduces to $\mathbf{u} = u(y)\hat{\mathbf{i}}$. Further, with in-plane deformation consideration

and unit vector constraint, the director further assumes a reformulated form as $\mathbf{n} = \sin \psi(y)\hat{\mathbf{i}} + \cos \psi(y)\hat{\mathbf{j}}$ where ψ represents the angle the director makes with the y axis. For nematic medium, the effective viscosity $\eta(\psi)$ depends on the director orientation resulting in the stress form $T_{12} = \eta(\psi)(du/dy)$. This casts the momentum equation as

$$\frac{d}{dy} \left[\eta(\psi) \frac{du}{dy} \right] = -a_p, \quad (6)$$

where the involved anisotropic viscosity reads [30]

$$\eta(\psi) = [2\alpha_1 \sin^2 \psi \cos^2 \psi + (\alpha_5 - \alpha_2) \cos^2 \psi + (\alpha_6 + \alpha_3) \sin^2 \psi + \alpha_4]/2. \quad (7)$$

Here α_1 to α_6 denote the Leslie viscosities. The solution to the above flow using no-slip condition at the channel wall and symmetric condition at the channel centerline reads

$$u = -a_p \left(\int_0^y \frac{ydy}{\eta(\psi)} - \int_0^H \frac{ydy}{\eta(\psi)} \right) = -a_p I_{C1}. \quad (8)$$

The corresponding average velocity (u_{av}) of the capillary front across the capillary cross section is estimated as $u_{av} = (1/H) \int_0^H u dy = (-a_p/H) \int_0^H I_{C1} dy = (-a_p/H) I_C$. Following the approach of the lumped-parameter model, the viscous force per unit wall breadth attributed to the shear stress at the walls then reads $F_{visc} = -2T_{12}|_{y=H}x$. Using Cauchy's equation of motion and replacing the pressure gradient with average velocity, we obtain the calculable form of the viscous force as $F_{visc} = -\frac{2H^2 x u_{av}}{I_C}$ where $I_C = \int_0^H I_{C1} dy = \int_0^H (\int_0^y [ydy/\eta(\psi)] - \int_0^H [ydy/\eta(\psi)]) dy$. Since the director orientation ψ varies in the presence of an electric field (attributed to the Fréedericksz transition [20,50]) which, in turn, alters the viscous properties, the phenomenon of electrorheology [9,51] is observed. In order to obtain a formal solution for the flow field and the resulting lumped viscous force, the director configuration $\psi(y)$ needs to be ascertained from the torque balance equation.

C. NLC director configuration

With the form of \mathbf{n} given above, the director torque equation for a NLC with one-constant elastic coefficient (K) reduces to [30]

$$K \frac{d^2 \psi}{dy^2} + \frac{1}{2} [\gamma_1 - \gamma_2 \cos(2\psi)] \frac{du}{dy} - \frac{1}{2} \varepsilon_0 \varepsilon_a E^2 \sin(2\psi) = 0. \quad (9)$$

Here $\gamma_1 = \alpha_3 - \alpha_2$ and $\gamma_2 = \alpha_3 + \alpha_2$ describes the viscosity coefficients while ε_a is the permittivity anisotropy given as $\varepsilon_a = \varepsilon_{\parallel} - \varepsilon_{\perp}$. Using $du/dy = -[a_p y/\eta(\psi)] = u_{av} H y/I_C \eta(\psi)$, we get

$$K \frac{d^2 \psi}{dy^2} + \frac{1}{2} [\gamma_1 - \gamma_2 \cos(2\psi)] \left(\frac{u_{av} H y}{I_C \eta(\psi)} \right) - \frac{1}{2} \varepsilon_0 \varepsilon_a E^2 \sin(2\psi) = 0. \quad (10)$$

This torque equation is complemented with strong planar anchoring conditions at the walls (i.e., at $y = \pm H$, $\psi = \pi/2$) and homeotropic condition at the NV interface.

D. Lumped-order formalism

The development of the capillary front along the longitudinal direction may now be fully described by the individual force balance per unit breadth in Eq. (1) as

$$\frac{d}{dt} \left(2H\rho x \frac{dx}{dt} \right) = 2\gamma_s \cos \theta_{\parallel\perp} + \frac{KC_{\parallel\perp}}{H} - 2H\rho g x + \frac{2H^2 x}{I_C} \frac{dx}{dt} \quad (11)$$

wherein we have replaced $\gamma_{s,\text{iso}}^{\text{NV}}$ by γ_s and u_{av} by the capillary front evolution (or entry) rate dx/dt . The corresponding director configuration is obtained from the torque balance equation. Before proceeding to state the solution procedure and obtaining the results of the above coupled equations, we first nondimensionalize the governing equations.

E. Nondimensionalization

We follow a dimensionless scheme using $\bar{x} = x/H$, $\bar{y} = y/H$, $\bar{t} = t/t_0$, and $\bar{\eta} = \eta/\eta_{\text{ref}}$ where the time and velocity scales are given as $t_0 = \sqrt{\rho H^3/\gamma_s}$ and $u_{\text{ref}} = H/t_0$. Identifying the above lumped forces and recognizing the coupled effect of electrocapillarity and elastic forces at the NV interface, the resulting dimensionless equation [corresponding to Eq. (11)] dictating the evolution of the capillary front (\bar{x}) with time (\bar{t}) reads

$$\frac{d}{d\bar{t}} \left(\bar{x} \frac{d\bar{x}}{d\bar{t}} \right) = \cos \theta_{\parallel\perp} + \frac{\text{Ea}_b}{2} - \text{Bo} \bar{x} + \frac{\text{Ca}}{\bar{I}_C} \bar{x} \frac{d\bar{x}}{d\bar{t}}, \quad (12)$$

where $\bar{I}_C = \int_0^1 \bar{I}_{C1} d\bar{y} = \int_0^1 (\int_0^{\bar{y}} [\bar{y} d\bar{y} / \bar{\eta}(\psi)] - \int_0^1 [\bar{y} d\bar{y} / \bar{\eta}(\psi)]) d\bar{y}$, $\theta_{\parallel\perp}$ is the effective contact angle of the capillary meniscus, and $\bar{\eta} = \eta/\eta_{\text{ref}}$ is the dimensionless anisotropic NLC viscosity. This viscosity depends on the director configuration (ψ) which is obtained from the torque balance equation that reads in dimensionless form [of corresponding Eq. (10)] as

$$\frac{d^2 \psi}{d\bar{y}^2} = \frac{\bar{q}}{2} \sin(2\psi) - \frac{\text{Er}}{2\bar{I}_C} [\bar{\gamma}_1 - \bar{\gamma}_2 \cos(2\psi)] \left(\frac{\bar{y} \bar{u}_{\text{av}}}{\bar{\eta}(\psi)} \right). \quad (13)$$

Here $\bar{u}_{\text{av}} = d\bar{x}/d\bar{t}$ denotes the average dimensionless velocity of the capillary front; $\bar{\gamma}_1$ and $\bar{\gamma}_2$ denote the dimensionless viscosity coefficients [30]. This torque equation is complemented with strong anchoring with planar conditions at the walls (i.e., at $\bar{y} = \pm 1$, $\psi = \pi/2$) and homeotropic conditions at the NV interface. To account for the effective surface energy due to the coupled influence of electric field and interfacial nematic elasticity, we nondimensionalize the modified the YL equation [Eq. (5)] to

$$\cos \theta_{\parallel\perp} - \frac{\text{Ea}_c}{2} \varphi_{E,\parallel\perp}^2 \sin \theta_{\parallel\perp} = \cos \theta_{\text{Ec}}, \quad (14)$$

where $\cos \theta_{\text{Ec}} = \cos \theta_c + \bar{q} \text{Ca}/\text{Er}$ and $\varphi_{E,\parallel\perp} = (\pi/2 - \theta_{\parallel\perp})/(\pi - \theta_{\parallel\perp})$. Besides the usual Bond number $\text{Bo} = \rho g H^2/\gamma_s$ and capillary number $\text{Ca} = \eta_{\text{ref}} H/\gamma_s t_0$ [48,52], a few other involved dimensionless physical parameters arising in the dimensionless formulation are Ericksen number $\text{Er} = H\eta_{\text{ref}} u_{\text{ref}}/K$, dielectric strength parameter $\bar{q} = \varepsilon_0 \varepsilon_a H^2 E^2/K$, $\text{Ea}_c = K/\gamma_s r_c$, and $\text{Ea}_b = KC_{\parallel\perp}/\gamma_s H$. Er denotes the relative strength of the viscous effects induced due to imposed flows in comparison to its elastic influences. As stated earlier, here we

shall primarily be concerned with low Er values that are more pertinent to flows through microconfinement.

Ea_b describes the importance of bulk elasticity-induced surface tension compared to the nematic-vapor interface tension. With $C_{\parallel\perp} \sim 1$, $K \sim 10^{-11}$ N, $\gamma_s \sim 10^{-2}$ N/m, it is clear that even for a micrometer-sized channel, the nematic-vapor interfacial energy far exceeds the long-range elastic induced surface tension [31] and hence, we neglect its effect hereafter. With r_c usually being in the order of 10 nm [53], $\text{Ea}_c \sim 0.1$ and, thus, interfacial effects due to long-range elasticity at the contact line must be accounted for. The dielectric strength parameter \bar{q} denotes the relative strength with which the electric field attempts to modify the director configuration compared to the medium elasticity that hinders such orientational changes. \bar{q} governs the amount of ER effect that the capillary system encounters either due to a stronger electric field or a larger dielectric anisotropy. We further discuss a few other relevant dimensionless numbers that may subtly arise in such a situation. The Reynolds number $\text{Re} = \rho U l/\mu$ ($U = H/t_0$) is defined as the ratio of the inertial forces to the viscous forces. With the given choice of the timescale $t_0 = \sqrt{\rho H^3/\gamma_s}$, it may easily be seen that Re is actually the inverse of the capillary number which is defined as $\text{Ca} = \eta_{\text{ref}} H/\gamma_s t_0$. Thus, as we observe for low Ca (or high Re) flows, the capillary front tends to oscillate about the Jurin height which is reminiscent of high inertial forces at play in such regimes. On the other hand, for high Ca (or low Re) flows, the viscous effects are dominating resulting in the suppression of the oscillatory regime. Froude number $\text{Fr} = U/\sqrt{gl}$ is defined as the ratio of inertia to gravity forces. Again, the Froude number is effectively the inverse of the Bond number defined as $\text{Bo} = \rho g H^2/\gamma_s$ for the choice of timescale. We further report the Ohnesorge number that is defined as the $\text{Oh} = \sqrt{\text{We}/\text{Re}}$, where We is the Weber number which implies the relative importance of inertial forces to surface tension forces ($\text{We} = \rho U^2 H/\sigma$). With the given choice of t_0 , We is in order of unity. Thus, Oh is the inverse of Re or Oh is equivalent to Ca in the present study. Therefore, it is observed that other relevant dimensionless numbers would appear through particular combinations of the numbers already appearing in the governing transport equation.

Post development of the governing equations and subsequent nondimensionalization, we move on to solving the coupled set of dimensionless equations [Eqs. (12)–(14)] using a numerical method. The numerical procedure followed is an iterative time-marching scheme. From an initial guess of ψ , the value of \bar{I}_C is obtained using which an updated $\bar{u}_{\text{av}} = d\bar{x}/d\bar{t}$ is estimated from Eq. (12). With the updated \bar{u}_{av} , the distribution of ψ is obtained from Eq. (13) and the process is followed. The value of ψ is obtained at every time step with an updated value of \bar{u}_{av} and the procedure is repeated until a steady state of the capillary front is reached.

III. RESULTS AND DISCUSSIONS

We proceed to solve the coupled governing equation as stated above using the properties of 5CB provided in Table I. From the property values, the rotational Leslie viscosity and torsion coefficient, respectively, has the value $\gamma_1 = \alpha_3 - \alpha_2 = 0.0777$ and $\gamma_2 = \alpha_3 + \alpha_2 = -0.0848$. The isotropic contact angle θ_c is independent of the orientation of the director

TABLE I. Physical properties of NLC 5CB (Chemical name: 4-cyano-4'-pentylbiphenyl).

Property	Value	Property	Value
Relative dielectric Permittivity	$\epsilon_{\parallel} = 18.5$ $\epsilon_{\perp} = 7$		$\alpha_1 = -0.0060$ $\alpha_2 = -0.0812$
		Leslie viscosity	$\alpha_3 = -0.0036$ $\alpha_4 = 0.0652$
Elastic constant (in pN)	$K = 6.2$		$\alpha_5 = 0.0640$ $\alpha_6 = -0.0208$

adjacent to the free interface and is found from the observed contact angle θ_{\perp} [Eq. (14)] in the absence of electric field. For 5CB, the value of the isotropic nematic-vapor surface tension is considered ~ 25 mN/m [54], while as a representative case, the isotropic contact angle is assumed to be 50° . We consider a capillary width varying within the order of 10^{-2} to 10^{-5} mm which helps us to characterize flows of high and low Bo regimes. Before showcasing the coupled electrocapillary and ER effect of the NLC medium, we attempt an experimental validation of the present formalism by comparing our results to previously performed experimental studies [29] related to NLC 5CB in the absence of any electric field.

A. Experimental perspective

In Fig. 2(a), we obtain the position of the capillary front (x) as a function of time (t) for a capillary cell with width $2H = 10.1 \mu\text{m}$ and the aforementioned NLC properties. The channel is treated with parallel rubbed polyimide which results in planar arrangement of the director at the NS interface. As observed, the predicted evolution of the capillary front agrees well with the experimental values. Further, the velocity of the capillary front found from experimental data closely matches with the present analysis. In Fig. 2(b), we show the capillary front velocity (\dot{x}) for two different capillary cell widths. It is seen clearly that for larger channel width, the front enters the capillary with a higher velocity as expected. The present analysis depicts considerable good agreement with the experimental results in the context of the capillary filling rate. We must note that the initial peak in capillary rise velocity, as shown in Fig. 2, is hard to capture

from experimental observations, and thus is excluded from the depiction.

Here, we specifically examine the flows through two different channel sizes; one where H is low and the inertial effect is negligible compared to viscous or surface tension effects transpiring in a low Bo regime and the other, where width H is in the order of $100 \mu\text{m}$ or larger and the inertial effects comes into prominence. Hence, Bo in the order of 10^{-6} for the former case and in the order of 10^{-2} for the latter case is considered. It must be appreciated that singling out and depicting the Bo variation will not effectively capture realistic situations since a change in Bo due to altering channel dimensions also results in a change in Er and Ca, simultaneously. Therefore, we note here that as Bo increases, Er rises while the value of Ca drops.

Next, we proceed to observe the individual effects of electric field or dielectric anisotropy (i.e., the effect of \bar{q}) on the director profile of the NLC. In Fig. 3(a), the individual effect of \bar{q} and Er on the director configuration is showcased in order to appreciate their individual influence to reorient the director across the channel width. It is noted that both of these parameters tend to orient the director toward a homeotropic alignment in the bulk but with different magnitude. With an increase in electric field or dielectric anisotropy (i.e., an increase in \bar{q}), the director profile tends to align completely toward the applied electric field which is transverse to the flow direction, thus resulting in a homeotropic configuration. On the contrary, with an increase in Er, the viscous torque tends to rotate the director to a particular angle, known as the Leslie angle, toward the flow indicating a shear thickening or shear thinning phenomenon, depending on the initial director configuration. To be precise, an initial director arrangement parallel to the flow direction leads to shear thickening effect, while an initial director arrangement perpendicular to the flow direction results in a shear thinning effect. Thus, as seen above in Fig. 3(a), as both these parameters are increased, the effective viscosity is enhanced since a homeotropiclike arrangement renders stronger hindrance to the fluid flow. However, the viscosity enhancement due to \bar{q} has more prominence than that observed due to Er.

Figure 3(b) depicts the effect of apparent viscosity due to the combined effects of the Ericksen number and \bar{q} variation. As seen from Fig. 3(b), as Er is attenuated, the effect of \bar{q}

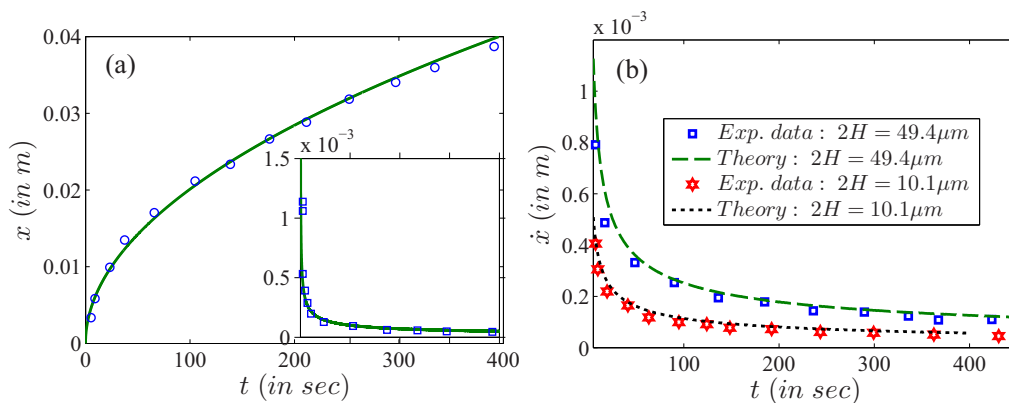


FIG. 2. The comparison between the semianalytical expressions of the present theory and previous experimental findings [29] for (a) capillary filling and filling rate and (b) filling rate through two different capillary pores of NLC 5CB medium in the absence of an external electric field.

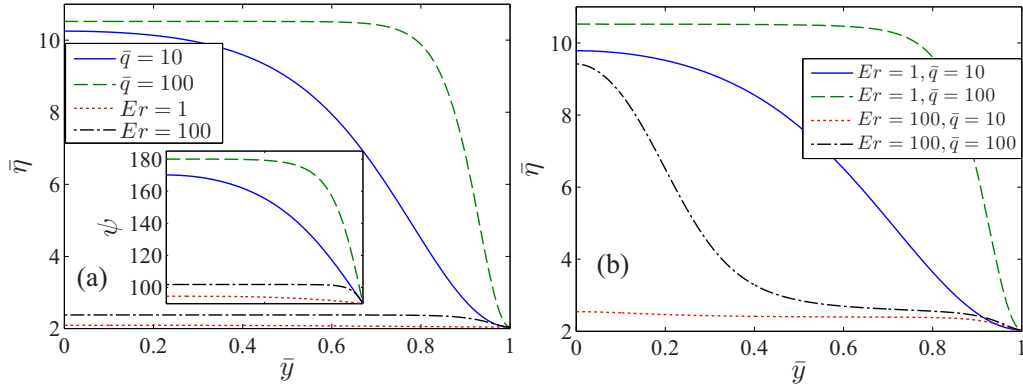


FIG. 3. Depicts the variation of (a) dimensionless viscosity and (inset) director angle as a function of the channel width for $Er = 1$ for varying \bar{q} and $\bar{q} = 10$ for varying Er . Plot (b) depicts the variation of gross viscosity as a function of the channel width for various combinations of the dielectric strength parameter \bar{q} and Ericksen number Er .

on the resulting effective viscosity is augmented resulting in a dominant ER effect. However, at higher Er , an increase in \bar{q} does not grossly change the effective viscosity, and thus the ER phenomenon is suppressed. In fact, it may be noteworthy that for large \bar{q} , an increase in Er exhibits shear thinning characteristics. Such contrasting characteristic regimes are typical of NLC medium and have been investigated in the literature [51,55–57]. These observations form the background for the results obtained from capillary dynamics estimation in the following figures.

In Fig. 4(a), we depict the capillary front propagation and its rate as a function of time for different values of \bar{q} . A direct observation is that the capillary front takes a longer time to develop in low Bo regimes. This trend will be consistent in low Bo regimes. The slowdown of the capillary filling process in narrower channels is attributed to the high viscous hindrance the flow encounters compared to flows through larger channels. We may further notice that the effect of \bar{q} on the capillary rise dynamics is effectively to enhance the viscous resistance to the filling process. Higher \bar{q} envisage a slower filling process attributed to the ER effect of the NLC medium as stated above. Although the above observation remains true for initial filling times, it is interestingly observed that at longer times the equilibrium height attained is higher for larger \bar{q} . This is simply

due to the fact that our formulations have effectively captured the electrocapillary effect due to which the contact angle decreases resulting in a larger Jurin height. Thus, as \bar{q} increases, the final Jurin height will always be higher. Figure 4(b) depicts a similar filling process but for high Bo flows. We note a higher filling rate resulting in the capillary front attaining the equilibrium Jurin height in less time. We further note that for high \bar{q} the capillary front realizes a higher Jurin height irrespective of the strong ER effect since the final height is independent of viscous drag. It is further observed that for such Bo flows, the capillary front experiences oscillations about the Jurin height which is typical for such regimes and has also been experimentally noted and theoretically predicted by numerous previous studies [48,52]. Another intriguing observation shows that as \bar{q} increases, the Jurin height simultaneously gets enhanced; however, the oscillations around the Jurin height get completely suppressed, attributed to the ER characteristic of the NLC fluid. In sharp contrast, for the Newtonian case a higher Jurin height, realized due to a stronger electrocapillary effect, is often associated with stronger oscillations for flows in high Bo number regimes. Thus, we see unusual characteristics for capillary filling dynamics of the anisotropic NLC medium in the presence of an electric field that enables modulation of Jurin height and entry rate attained by the capillary front.

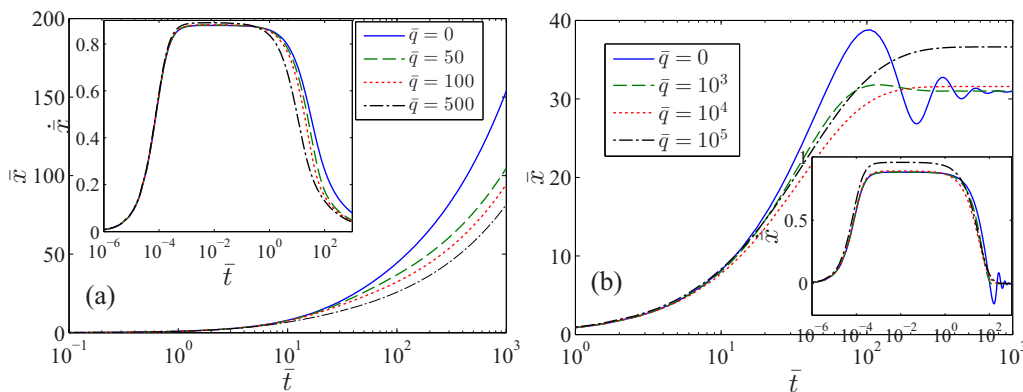


FIG. 4. The capillary front propagation and its rate as a function of dimensionless time for different values of the dielectric strength parameter \bar{q} for (a) $Bo = 10^{-6}$ and (b) $Bo = 0.02$. The other dimensionless parameters involved are for case (a) $Ca = 0.01$, $Er = 20$, and $Ea_c = 5$ and (b) $Ca = 0.002$, $Er = 100$, and $Ea_c = 5$.

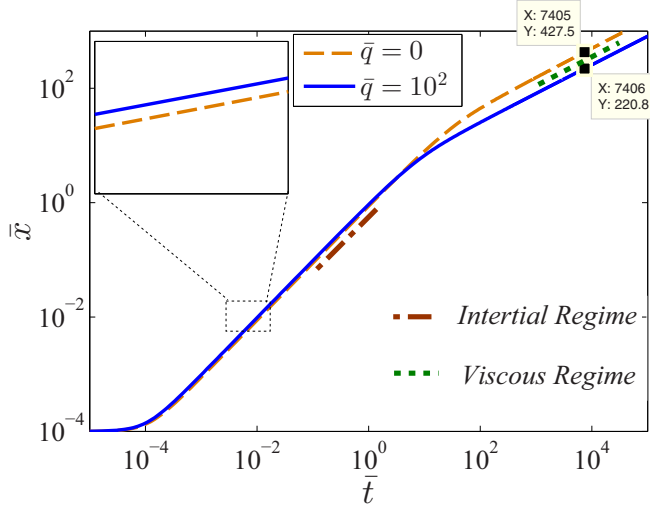


FIG. 5. Depicts the different capillary filling regimes for the NLC medium. The approximations from the scaling analysis are compared to the numerical solution for two values of \bar{q} . The other parameters for the present case include $Bo = 10^{-6}$, $Ca = 0.01$, $Er = 20$, and $Ea_e = 5$.

B. Scaling analysis

Here we attempt to bring about a simplified scaling analysis for the capillary filling regimes under the influence of the induced ER effect. For capillary filling dynamics, the initial fluid rise is governed by the balance between the inertial and surface tension forces. This leads to the classical inertial regime where the timescales with capillary front displacement (i.e., $\bar{x} \sim \bar{t}$ or $\dot{x} \sim 1$). This initial regime, as seen in Fig. 5, has been elaborately investigated in numerous previous studies [48]. Post inertial regime, the capillary front encounters the Washburn regime [47]. Here the surface tension force is balanced by the viscous force resulting in the form $\bar{t} \sim \bar{\eta}_{\text{eff}} \bar{x}^2$ that validates the classical scaling as $\bar{x} \sim \sqrt{\bar{t}}$, which is also observable in Fig. 5. From here on, the scaled form simply transpires to $\frac{1}{2}[\log(\bar{\eta}_{\text{eff}}) + \log(\bar{t})] \sim \log(\bar{x})$ where $\bar{\eta}_{\text{eff}}$ is the scaled viscosity and a function of \bar{q} . From Fig. 5 we notice that the difference in the y intercept of the two plots for different \bar{q} is given by $\log_{10}(427.5) - \log_{10}(220.8) \cong 0.29$.

The parameter \bar{q} is primarily responsible for the ER effect, which is in turn governed by the director deformation that occurs beyond the Fréedericksz transition electric field. This deformation alters the effective viscosity of the fluid medium. Thus, to perform the scaling analysis, we look toward the estimation of an approximate director configuration, and in turn, viscosity as a function of \bar{q} . As an approximate consideration, here we neglect the viscous effects due to low Er [Eq. (13)] and analytically describe the director configuration solely due to the applied electric field. The maximum angular deformation ψ_m of the director is then found from its relation with \bar{q} given by [30]

$$\sqrt{\bar{q}}/2 = JI_C(\psi'_m) = \int_0^{\pi/2} \frac{d\varphi'}{\sqrt{1 - [\sin(\psi'_m) \sin(\varphi')]^2}}, \quad (15)$$

where JI_C represents the complete Jacobi elliptic function of the first kind with modulus angle ψ'_m and $\psi'_m = \pi/2 - \psi_m$. With known ψ_m , $\bar{y}'\sqrt{\bar{q}} = \int_0^\varphi d\varphi'/\sqrt{1 - [\sin(\psi'_m) \sin(\varphi')]^2} = JI_C(\varphi', \bar{y}', \psi'_m)$ describes the director configuration across the channel, where JI_C represents the incomplete Jacobi elliptic function of first kind with modulus angle ψ'_m and argument \bar{y}' (\bar{y}' being the rescaled \bar{y} from 0 to 1). The director angle then reads $\psi = \pi/2 - \sin^{-1}[\sin(\varphi') \sin(\psi'_m)]$. With this distribution, we obtain the approximate effective viscosity from $\bar{\eta}_{\text{eff}} = \int_0^1 \bar{\eta}(\psi) d\bar{y}$. Here we observe that for \bar{q} having values 0 and 100, the y-intercept difference approximately again equals $\log(\bar{\eta}_{\text{eff}})|_{\bar{q}=0} - \log(\bar{\eta}_{\text{eff}})|_{\bar{q}=100} \cong 0.31$. The slight discrepancy from the value 0.29 is attributed to neglecting the viscous torque effects on director deformations. Therefore, besides capturing the two classical regimes of capillary filling, the present scaling also explicitly encases the implications of the ER phenomenon expressed due to the electric-field-induced Fréedericksz transition. We now understand that this ER phenomenon is effectively dictated by the surface anchoring and dielectric anisotropy of the NLC director. As mentioned earlier, the surface anchoring of NLCs is easily controllable through various surface treatments. Even the dielectric and conductivity anisotropy may be subjected to modulation by proper combination of two or more NLCs in a medium [11,58,59]. In the present case, a planar anchoring and positive dielectric anisotropy is assumed (for a representative case for 5CB) which is responsible for the ER effect. Instead, a negative (or zero) anisotropy would make the fluid electrorheologically inactive rendering classical Newtonian characteristics to the flow. Thus, the ER activity and its strength, dictated by the combination of surface properties and dielectric anisotropy, may be set beforehand, thereby obtaining the desirable modulation capability of the NLC dynamics.

IV. CONCLUSIONS

In summary, the present study couples the intrinsic ER and electrocapillary effect along with the inherent anisotropy of complex NLC to investigate its dynamics through a parallel-plate confinement. It showcases the two-way coupling of director orientation and resulting capillary front velocity in the presence of a transverse electric field by employing a reduced-order approach. Interestingly, it is seen that the electric field presence, although it slows down the capillary filling process, generates the intrinsic electrocapillary phenomenon resulting in an enhanced Jurin height attainment. The capillary filling rate is also dependent on the counterbalancing influences of aiding electrocapillary forces and the hindering electrorheological effects. Thus, despite attaining a higher Jurin height due to stronger electrocapillary force (or stronger applied electric field), the rate of attainment of such equilibrium Jurin height is slower. This observable characteristic is quite contrary to capillary filling studies involving non-ER Newtonian or non-Newtonian fluids wherein electrocapillarity augments the capillary entry rate [60,61]. Further, the effect of shear thinning as well as shear thickening rheology of the fluid depending on the initial director configuration is observed which additionally lends a better modulation capability to the present system. We later on examined the oscillatory behavior of the capillary front at high

Bo flows. Finally a scaling analysis of the filling process is accomplished where two regimes are recognized while the ER effect in the viscous regime has been successfully scaled to the reorientation of the director in the presence of the electric field.

It is additionally noteworthy that an application of an oscillating electric field instead of a constant one will simultaneously affect the favorable electrocapillary force as well as the adverse viscous force induced via the ER phenomenon. Since the driving (favorable) electrocapillary force may follow a particular frequency equal to the oscillating frequency of the applied electric field, resonance may be observed in the capillary oscillation regimes [62–64]. Besides, one may also employ oscillating capillary walls leading to peristaltic transport of the capillary front which may further induce

resonant oscillations [65,66] in the capillary front oscillatory regimes. These resonating conditions may certainly enhance the peak attained by the climbing capillary surface (front) and stands as an exciting alternative to flow modulation through narrow conduits. However, it must be noted that the final Jurin height (or time-averaged Jurin height) remains independent of the oscillating frequency and is only a function of the electric field strength, the surface anchoring conditions, and the surface tension effects. Thus, we infer that these tunable parameters may be effectively exploited to modulate the overall capillary filling dynamics of NLCs, bearing far-reaching implications toward an improved design of electro-optical systems, electrorheological utilities, electrokinetic flow control, as well as biomedical microdevices.

-
- [1] A. Sengupta, in *Topological Microfluidics* (Springer, Cham, 2013), pp. 83–135.
- [2] A. Sengupta, *Liq. Cryst. Today* **24**, 70 (2015).
- [3] A. Safrani, M. Abuleil, S. Isaac, A. Solodar, I. Klapp, M. G. Kirzhner, and I. Abdulhalim, in *SPIE Newsroom*, edited by I. C. Khoo (2014), p. 91820R.
- [4] J. P. F. Lagerwall and G. Scalia, *Curr. Appl. Phys.* **12**, 1387 (2012).
- [5] J. F. Algorri, V. Urruchi, N. Bennis, J. M. Sánchez-Pena, and J. M. Otón, *Opt. Express* **23**, 13899 (2015).
- [6] A. Inoue and S. Maniwa, *J. Appl. Polym. Sci.* **55**, 113 (1995).
- [7] C. I. Mendoza, A. Corella-Madueño, and J. A. Reyes, *Phys. Rev. E* **77**, 011706 (2008).
- [8] A. D. Guillén and C. I. Mendoza, *J. Chem. Phys.* **126**, 204905 (2007).
- [9] J. C. Medina and C. I. Mendoza, *Europhys. Lett.* **84**, 16002 (2008).
- [10] M. De Volder, K. Yoshida, S. Yokota, and D. Reynaerts, *J. Micromech. Microeng.* **16**, 612 (2006).
- [11] I. Lazo, C. Peng, J. Xiang, S. V. Shiyankovskii, and O. D. Lavrentovich, *Nat. Commun.* **5**, 5033 (2014).
- [12] I. Lazo and O. D. Lavrentovich, *Philos. Trans. R. Soc., A* **371**, 20120255 (2013).
- [13] M. G. Tomilin, S. A. Povzun, A. F. Kurmashev, E. V. Gribanova, and T. A. Efimova, *Liq. Cryst. Today* **10**, 3 (2001).
- [14] Y.-H. Lin, in *The Current Trends of Optics and Photonics*, 129th ed. (Springer, Dordrecht, 2015), pp. 337–354.
- [15] S. J. Woltman, G. D. Jay, and G. P. Crawford, *Nat. Mater.* **6**, 929 (2007).
- [16] G. De Luca and A. D. Rey, *J. Chem. Phys.* **127**, 104902 (2007).
- [17] M. Ravnik and J. M. Yeomans, *Phys. Rev. Lett.* **110**, 026001 (2013).
- [18] T. B. Jones, *Langmuir* **18**, 4437 (2002).
- [19] P. Sheng and W. Wen, *Annu. Rev. Fluid Mech.* **44**, 143 (2012).
- [20] P. G. de Gennes and J. Prost, *The Physics of Liquid Crystals*, 2nd ed. (Clarendon Press, Oxford, 1993).
- [21] N. Fries and M. Dreyer, *J. Colloid Interface Sci.* **320**, 259 (2008).
- [22] A. Hamraoui and T. Nylander, *J. Colloid Interface Sci.* **250**, 415 (2002).
- [23] F. Chauvet, S. Geoffroy, A. Hamoumi, M. Prat, and P. Joseph, *Soft Matter* **8**, 10738 (2012).
- [24] T. Andruk, D. Monaenkova, B. Rubin, W.-K. Lee, and K. G. Kornev, *Soft Matter* **10**, 609 (2014).
- [25] P. Joos, P. Van Remoortere, and M. Bracke, *J. Colloid Interface Sci.* **136**, 189 (1990).
- [26] G. Martic, F. Gentner, D. Seveno, D. Coulon, J. De Coninck, and T. D. Blake, *Langmuir* **18**, 7971 (2002).
- [27] R. M. Digilov, *Langmuir* **24**, 13663 (2008).
- [28] J. Dhar, U. Ghosh, and S. Chakraborty, *Soft Matter* **11**, 6957 (2015).
- [29] X.-D. Mi and D.-K. Yang, *Phys. Rev. E* **58**, 1992 (1998).
- [30] I. W. Stewart, *The Static and Dynamic Continuum Theory of Liquid Crystals: A Mathematical Introduction* (CRC Press, London/New York, 2004).
- [31] A. D. Rey, *Langmuir* **19**, 3677 (2003).
- [32] V. A. Tsvetkov, O. V. Tsvetkov, and V. A. Balandin, *Mol. Cryst. Liq. Cryst. Sci. Technol., Sect. A* **329**, 305 (1999).
- [33] J. Ignés-Mullol, J. Baudry, and P. Oswald, *Phys. Rev. E* **63**, 031701 (2001).
- [34] I. B. Liu, M. A. Gharbi, V. L. Ngo, R. D. Kamien, S. Yang, and K. J. Stebe, *Proc. Natl. Acad. Sci. USA* **112**, 6336 (2015).
- [35] J. A. Reyes and P. Palfy-Muhoray, *Phys. Rev. E* **58**, 5855 (1998).
- [36] M. Urbanski, C. G. Reyes, J. Noh, A. Sharma, Y. Geng, V. Subba Rao Jampani, and J. P. F. Lagerwall, *J. Phys.: Condens. Matter* **29**, 133003 (2017).
- [37] A. Sengupta, B. Schulz, E. Ouskova, and C. Bahr, *Microfluid. Nanofluidics* **13**, 941 (2012).
- [38] A. Sengupta, S. Herminghaus, and C. Bahr, *Liq. Cryst. Rev.* **2**, 73 (2014).
- [39] T. Stieger, M. Schoen, and M. G. Mazza, *J. Chem. Phys.* **140**, 54905 (2014).
- [40] G. Tóth, C. Denniston, and J. M. Yeomans, *Phys. Rev. Lett.* **88**, 105504 (2002).
- [41] C. Liu and M. C. Calderer, *SIAM J. Appl. Math.* **60**, 1925 (2000).
- [42] M. C. Calderer and B. Mukherjee, *Liq. Cryst.* **22**, 121 (1997).
- [43] M. C. Calderer, *Eur. J. Appl. Math.* **8**, 301 (1997).
- [44] J. A. Reyes, O. Manero, and R. F. Rodríguez, *Rheol. Acta* **40**, 426 (2001).
- [45] K. Negita, *J. Chem. Phys.* **105**, 7837 (1996).
- [46] J. A. Reyes, A. Corella-Madueño, and C. I. Mendoza, *J. Chem. Phys.* **129**, 84710 (2008).
- [47] E. W. Washburn, *Phys. Rev.* **17**, 273 (1921).
- [48] S. Das and S. K. Mitra, *Phys. Rev. E* **87**, 063005 (2013).

- [49] A. Bandopadhyay, U. Ghosh, and S. Chakraborty, *Phys. Rev. E* **89**, 053024 (2014).
- [50] V. Fréedericksz and V. Zolina, *Trans. Faraday Soc.* **29**, 919 (1933).
- [51] J. Dhar and S. Chakraborty, *Phys. Fluids* **29**, 92008 (2017).
- [52] J. Dhar, P. Jaggi, and S. Chakraborty, *RSC Adv.* **6**, 60117 (2016).
- [53] E. R. Soulé and A. D. Rey, *Soft Matter* **8**, 1395 (2012).
- [54] M. G. J. Gannon and T. E. Faber, *Philos. Mag. A* **37**, 117 (1978).
- [55] P. D. Olmsted and C.-Y. D. Lu, *Phys. Rev. E* **60**, 4397 (1999).
- [56] M. E. Cates and S. T. Milner, *Phys. Rev. Lett.* **62**, 1856 (1989).
- [57] C. Denniston, E. Orlandini, and J. M. Yeomans, *Europhys. Lett.* **52**, 481 (2000).
- [58] N. Trbojevic, D. J. Read, and M. Nagaraj, *Phys. Rev. E* **96**, 052703 (2017).
- [59] M. Schadt and F. Muller, *IEEE Trans. Electron Devices* **25**, 1125 (1978).
- [60] M. W. J. Prins, *Science*. **291**, 277 (2001).
- [61] R. C. Gough, A. M. Morishita, J. H. Dang, M. R. Moorefield, W. A. Shiroma, and A. T. Ohta, *Micro Nano Syst. Lett.* **3**, 4 (2015).
- [62] J. Olson, C. Ursenbach, V. I. Birss, and W. G. Laidlaw, *J. Phys. Chem.* **93**, 8258 (1989).
- [63] V. Vogel and D. Moebius, *Langmuir* **5**, 129 (1989).
- [64] J. M. Oh, S. H. Ko, and K. H. Kang, *Langmuir* **24**, 8379 (2008).
- [65] J. Ogawa, I. Kanno, H. Kotera, K. Wasa, and T. Suzuki, *Sens. Actuators, A* **152**, 211 (2009).
- [66] M. Hilpert, D. Stopper, and G. H. Jirka, *Z. Angew. Math. Phys.* **48**, 424 (1997).